Coulomb blockade: Toward charge control of self-assembled GaN quantum dots at room temperature

C A Sgroi, J. Brault, J.-Y. Duboz, S. Chenot, P. Vennéguès, A. Ludwig, A D Wieck

▶ **To cite this version:**

C A Sgroi, J. Brault, J.-Y. Duboz, S. Chenot, P. Vennéguès, et al.. Coulomb blockade: Toward charge control of self-assembled GaN quantum dots at room temperature. Applied Physics Letters, 2022, 120 (1), pp.012105. 10.1063/5.0073864 . hal-03828253

HAL Id: hal-03828253
https://cnrs.hal.science/hal-03828253

Submitted on 16 Dec 2022

HAL is a multi-disciplinary open access archive for the deposit and dissemination of scientific research documents, whether they are published or not. The documents may come from teaching and research institutions in France or abroad, or from public or private research centers.

L'archive ouverte pluridisciplinaire **HAL**, est destinée au dépôt et à la diffusion de documents scientifiques de niveau recherche, publiés ou non, émanant des établissements d'enseignement et de recherche français ou étrangers, des laboratoires publics ou privés.

Coulomb blockade: Towards charge control of self-assembled GaN quantum dots at room temperature

C. A. Sgroi,[1] J. Brault,[2] J-Y Duboz,[2] S. Chenot,[2] P. Vennéguès,[2] A. Ludwig,[1] and A. D. Wieck[1]
[1)] *Chair of Applied Solid State Physics, Ruhr-Universität, 44780 Bochum, Germany*
[2)] *Université Côte d'Azur, CNRS, CRHEA, Rue Bernard Gregory, 06560 Valbonne, France*

(*Electronic mail: carlo.sgroi@ruhr-uni-bochum.de)

(Dated: 26 November 2021)

We present Capacitance-Voltage (C(V)) measurements of self-assembled wurtzite-GaN quantum dots (QDs). The QDs are embedded in a charge-tunable diode structure and were grown by molecular beam epitaxy (MBE) in the Stranski-Krastanov growth method. The internal electric fields present in GaN and its alloys together with its wide bandgap make this material system an ideal candidate for high-temperature quantum applications. Charges and the internal electric fields influence the energy spacing in the QDs. We correlate photoluminescence measurements with C(V) measurements and show single-electron charging of the QDs and a Coulomb blockade energy of around 70 meV at room temperature. This finding demonstrates the possibility of quantum applications at room temperature.

Quantum dots (QDs) have opened a new dimension in semiconductor physics and technology research due to their atom-like energy structure. They are already used in applications such as QLEDs[1] and quantum information technology applications are within reach.[2] Single charge quanta control via a Coulomb blockade plays a significant role in stabilizing the emission and eliminating the blinking of GaAs QDs for quantum photonics.[3] However, applications as quantum bits in GaAs-based alloys are so far limited to low temperatures of about T < 20 K.[4] GaN and its alloys, in contrast, have properties that make them ideal candidates for high-power and high-temperature microelectronic and QD storage devices[5,6], such as their excellent mechanical and thermal stability, high thermal conductivity, wide bandgap and large confinement energies. Commercial applications for GaN-based systems can be found in light emitting diodes and semiconductor lasers. Furthermore, huge progress in single-photon sources operational at ambient temperatures using QDs has been made.[7–9] Due to repulsive Coulomb interactions, charging of QDs in, e.g., diode structures, is accompanied by an additional energy to the ground state, called the Coulomb blockade energy. This effect can be used to realize quantum electronic applications. Coulomb blockade has been observed in GaN nanostructures in several studies before: At a temperature of up to 3 K, Coulomb oscillations were observed in a quantum point contact forming a GaN single-electron transistor.[10] Coulomb blockade with a single electron charging energy of 10 meV at 12 K was found in a self-assembled GaN QD.[11] In a double barrier GaN-nanostructure and a temperature regime of up to 35 K, a Coulomb blockade energy of 10 meV was measured.[12] The low Coulomb blockade in these studies originate from large-size QDs. Though electron charging at higher temperatures has been observed in Ge QDs in p-silicon substrates[13] and electron tunneling with storage in nano-crystalline silicon floating gate double-barrier structure[14], single-electron charging at ambient temperatures was not resolvable in these measurements. This contribution shows single-electron charging of self-assembled w-GaN QDs in a charge-tunable heterostructure at room temperature via capacitance-voltage (C(V)) spectroscopy. To the best of our knowledge, a Coulomb blockade energy has not been reported so far at room temperature. The findings in this study demonstrate the applicability for future quantum applications and devices at ambient temperatures.

The sample was grown by molecular beam epitaxy on a (0001) sapphire substrate. Ammonia was used as the nitrogen source and at a flow rate of 50 sccm, whereas solid sources were used for Ga, Al, and Si. At first, a 30nm-thick GaN buffer layer was grown at 450°C followed by a 150-nm thick AlN layer at 900°C. The diode structure begins with a 700 nm Si-doped $Al_{0.4}Ga_{0.6}N$ layer at 840°C for the back contact with a doping concentration of $2 \times 10^{18}\ cm^{-3}$. A 13 nm $Al_{0.4}Ga_{0.6}N$ layer then follows as the tunneling barrier, separating the back contact from a layer of self-assembled GaN QDs. The QDs are grown in a modified Stranski-Krastanov method with a two-dimensional (2D) GaN growth mode followed by a 3D island formation during a growth interruption under vacuum. The 2D GaN layer, the wetting layer (WL), consists of the pseudomorphic first monolayers which are lattice-matched grown and wetten the surface. Above this WL, the QD formation takes place. The GaN deposited amount is about 2 nm (equivalent to 8 monolayers), and the QD density of about $1 \times 10^{11}\ cm^{-2}$.[15] On top follows a 90 nm $Al_{0.4}Ga_{0.6}N$ layer as an insulating spacer and a 3 nm GaN cap layer for chemical stability. More details can be found in reference[16]. The back contact consists of Ti/Al/Ni/Au. Ni/Au gates with an area of $2 \times 10^{-4}\ cm^2$ on top of the sample form a Schottky contact with a Schottky barrier of 1.05 eV[17]. This charge-tunable diode structure allows C(V) spectroscopy[18] measurements. For this, we use an SR850 lock-in amplifier and apply a superimposed 10 mV AC and sweep DC signal to the sample gate and measure the AC amplitude at the back contact, which gives us the differential capacitance. The sample is mounted in a He closed-cycle cryostat (company Trans-MIT) for temperature-dependent measurements.

The excitonic energy states of the GaN QDs are shown in the PL measurement in Figure 1a. The peaks labeled as s and p correspond to the ground state and the first excited excitonic state of the main QD ensemble. The small shoulder labeled s_{sub} on the lower energy side of the spectrum indicates larger-sized QDs, which we identify as a subensemble[19]. The broadening of the s-peak indicates a hidden peak p_{sub} originating

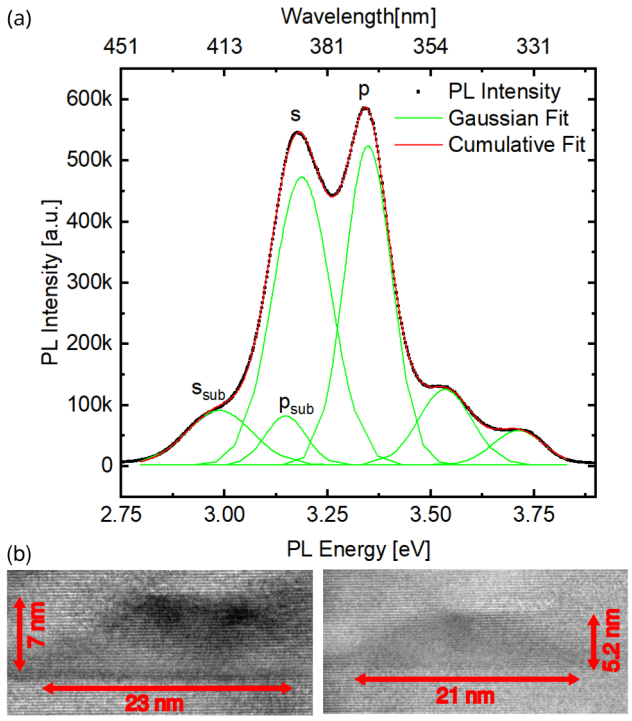

FIG. 1. (a) PL spectrum at 300 K of the sample N2189 (dotted black line). The peaks are labeled according to the energy states for the GaN QDs with the corresponding gaussian fit in green. The red line is the cumulative fit. (b) HRTEM images of a QD from the subensemble (left) and the main ensemble (right), respectively. The red bars give the lateral and horizontal dimension.

TABLE I. Energy spacing between quantum states in the PL and from one-dimensional simulation in the effective-mass approximation with $\Delta(s_{sub},s) = E(s) - E(s_{sub})$ and $\Delta(s_{sub},p_{sub}) = E(p_{sub}) - E(s_{sub})$.

	$\Delta(s_{sub},s)$	$\Delta(s_{sub},p_{sub})$
PL at 300 K	210 meV	150 meV
Simulation at 300 K	193 meV	195 meV

from the subensemble, which correlates to the subensemble's p-state. We fit the spectrum with Gaussians for the ensemble and subsensemble accordingly. The peak energy position differences from the PL and simulation for s, s_{sub} and p_{sub} are shown in Table I. The energy shift of the QDs is related to the quantum confined stark effect[20] due to the difference in height of the ensemble and subensemble.

Figure 1b shows HRTEM images of GaN QDs assigned to the subensemble (left) and the main ensemble (right). In agreement with previous studies[21], the QDs have the shape of a truncated pyramid with average dimensions of 5 nm height and 20 nm diameter for the main ensemble. For the subensemble, an average size of 7 nm in height and 25 nm in diameter are measured. The QD height is crucial for the energy confinement and energy spacing due to the internal electric field.[22,23]

Figure 2a shows a one-dimensional band structure simulation along the growth direction z, at different cross sections

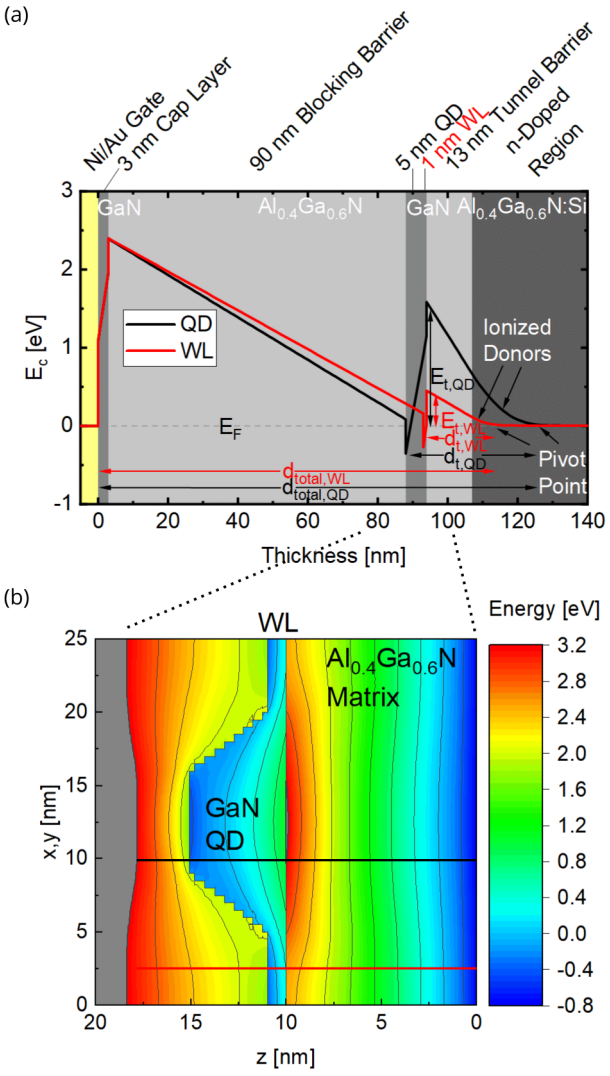

FIG. 2. (a) One-dimensional simulated band structure profile of the sample N2189 at 300 K with a QD (black) and WL (red) without applied gate voltage, simulated with Nextnano[24]. The sample heterostructure is shown colored in the background. Total distance d_{total}, tunnel distance d_t, and tunnel barrier height E_t are indicated for the quantum dot and WL, respectively. Region of ionized donors over the conduction band and the pivot points are indicated. (b) Nextnano simulated contour plot of a truncated pyramidal shaped GaN QD in an $Al_{0.4}Ga_{0.6}N$ matrix. The red and black line indicate the cross section of the simulation from Figure 2a for the WL and QD, respectively.

in the x,y-plane (see Figure 2b for the two-dimensional simulation of the QD and the $Al_{0.4}Ga_{0.6}N$ matrix). One of a QD (black line) and the other only the WL (red line). The main difference between the two lies in the barrier thickness d_t to the back contact and the barrier height E_t. Due to the internal electric fields present in the structure, the barrier formed by the $Al_{0.4}Ga_{0.6}N$ conduction band is thicker and higher at the QD position than outside the QD position. Compared to the WL potential, the QD potential is shifted to lower energies

and further away from the back contact: the distance $d_{t,QD}$ between the QD and the back contact is larger than the distance $d_{t,WL}$ of the WL to the back contact. The voltage scale can be converted into an energy scale via the linear lever arm approximation[25], expressed as:

$$E = \lambda^{-1} e(V_{bi} - V_G), \quad (1)$$

where e is the elementary charge, V_{bi} is the Schottky barrier height, V_G is the applied gate voltage and $\lambda = \frac{d_{total}}{d_t}$, the lever arm.

Figure 3a shows bidirectional C(V) measurements on the same sample as in Figure 2 at temperatures ranging from 150 K to 300 K. The arrows below and above the curves indicate the sweep direction of the gate voltage. For low temperatures (up to 200 K), the capacitance smoothly increases with bias across the whole gate voltage sweep, reflecting the change of the depletion width and charging of the back contact. With increasing temperatures, two things change. First, the whole capacitance curve shifts towards a higher value indicating a reduction in coupling distance to the back contact. Second, a distinct hysteresis arises. At intermediate temperatures (250 K), the hysteresis is highest. The forward sweep (left to right) shows a rapid increase of the capacitance at around 0.2 V. This signal originates from the charging of the QDs through the WL. The backward sweep (right to left) instead shows three peaks, which we attribute to the discharging signals from the QDs. For high temperatures (300 K), the QD charging (forward sweep) through the WL occurs at lower biases (-0.25 V) due to thermal activation. The discharging (reverse sweep) remains about the same in this bias range so that the hysteresis decreases. The backward sweep signal subtracted from the forward sweep signal is plotted in the inset of Figure 3a for improved visibility and fitting. The 250 K signal (green) with the highest hysteresis is shown in bold. Four peaks can be discerned with rising temperatures up to 250 K, at which point their height decreases. Furthermore, peak 4 disappears due to the WL charging shift towards lower gate voltages with rising temperature. In Figure 3b, the spectrum at 250 K is fitted with Gaussian peaks. We attribute peak 1 to the lowest energetic states of the subensemble with the larger dimensions and Peak 2 and 3 with the larger signal to the lowest energetic states s_1 and s_2 of the main ensemble. An additional energy separates the s-states, the Coulomb blockade energy[26], to charge the QD with a second electron. Since the same Coulomb repulsion applies to the subensemble as well, peak 1 is attributed to s_{1sub} and a hidden peak s_{2sub} underneath peak 2. Peak 4 must then originate from the next lowest energy state, which is the p_{1sub} state of the subensemble. In Figure 3c, we evaluate the integrated peak area, which reflects the measured charge, from our fits in Figure 3b. For the s-states, we observe a maximum at 250 K for both, the subensemble and main ensemble. The p_{1sub} signal appears to be partially suppressed from the WL signal as reflected in the low charge. The p_{1sub} signal shows no such temperature dependence like the s-states. We calculate the measured QD density from the single charge density with respect to the gate area A. Here, we focus on the signal at 250 K, as it is the most prominent signal. Considering the s-states of the subensemble and main

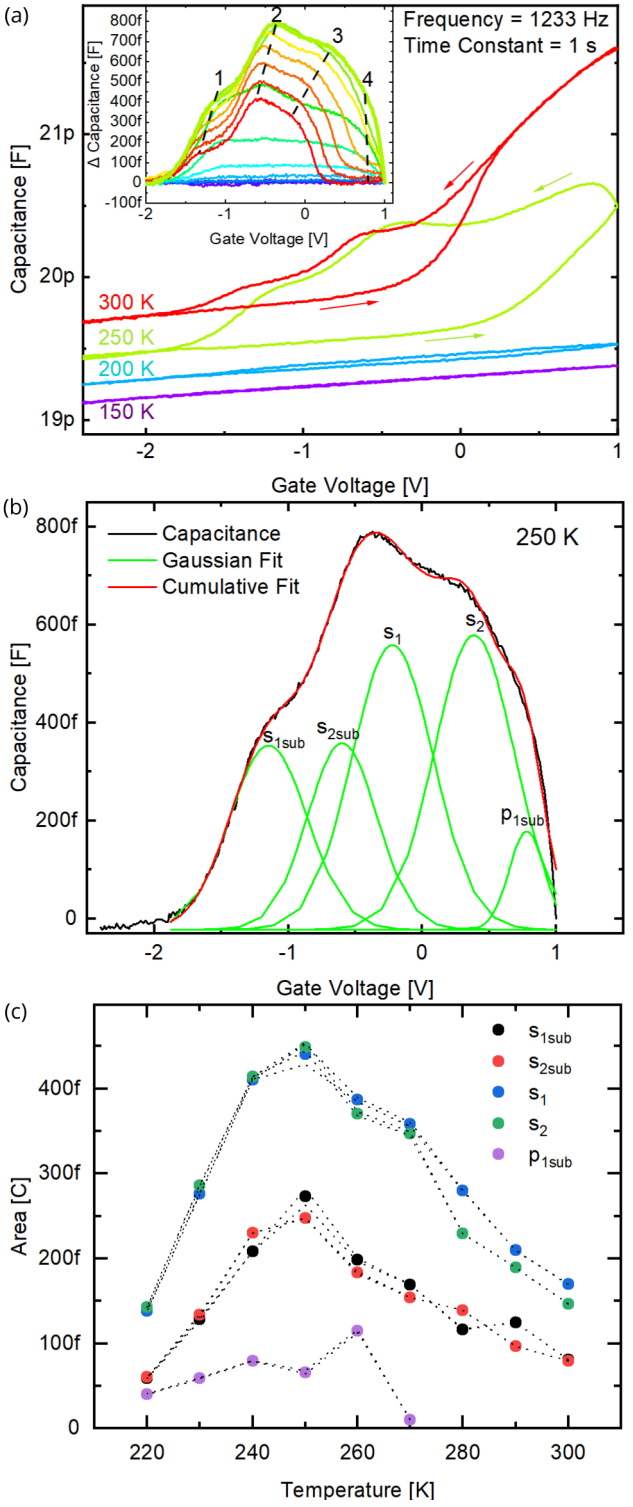

FIG. 3. (a) Temperature dependent C(V) measurement with bidirectional (arrows for sweep direction) gate sweep shown for 150, 200, 250, and 300 K. The inset shows the backward sweep subtracted from the forward sweep. (b) Gaussian fitted spectrum with each QD-state (green) for the 250 K signal (black) and the cumulative signal (red) from the fits. (c) The integrated area of each peak fit, from Fig. 3a (inset), is shown for temperatures between 220 K and 300 K in 10 K steps.

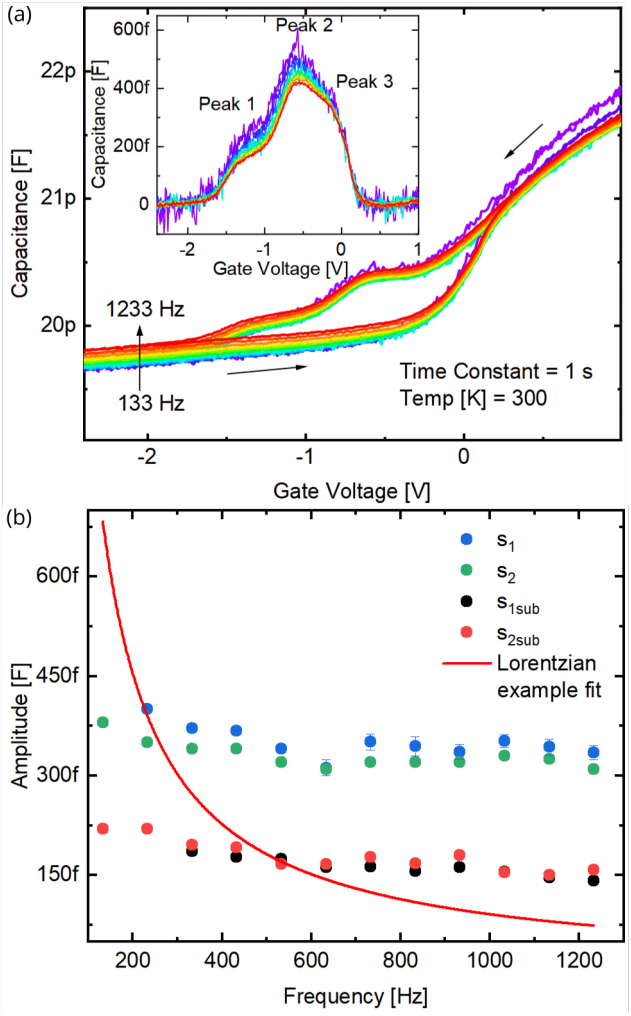

FIG. 4. (a) Bidirectional (arrows for sweep direction) frequency-dependent C(V) measurement from 133 Hz to 1233 Hz in 100 Hz steps. The inset shows the differential spectra of the forward and backward sweep. (b) Frequency-dependent amplitude of the fitted difference spectrum for each s-state and a Lorentzian example fit (red line).

ensemble, we measured a total charge Q of 2.85×10^{10} C and 5.73×10^{10} C, respectively. Dividing the total charge Q by a factor of two, due to the two electrons, by the gate area A and considering the corresponding lever arm λ of 4.1 for the main ensemble and 3.5 for the subensemble, we obtain a QD-density ρ_{QD} of:

$$\rho_{QD} = \frac{Q_{main}\lambda + Q_{sub}\lambda_{sub}}{2eA} = 8.6 \times 10^{10}\ cm^{-2}, \qquad (2)$$

in accordance with the estimated QD-density from a reference sample of around 1×10^{11} cm^{-2}. This confirms our assignment of single-electron charging for each peak. To further investigate the QD signal, we conducted a frequency-dependent C(V) measurement at 300 K shown in Figure 4a, ranging from 133 Hz to 1233 Hz, with the difference spectrum (backward sweep subtracted from the forward sweep) in the inset. According to previous studies[27,28], the peak heights of the C(V) spectra should follow a Lorentzian dependence on frequency. However, here, we have a much weaker frequency dependence than the Lorentzian dependence, as depicted in Figure 4b.

These measurements show a thermally activated process due to the strong temperature dependence and the freeze-out at lower temperatures. Moreover, the coupling between the QDs and the back contact is not a matter of pure tunnel coupling due to the non-Lorentzian frequency dependence as indicated in Figure 4b. Therefore, we propose a model employing an additional donor-assisted coupling and an intermediate WL transfer state. A schematic of the conduction band and its simplified quantum states of the WL and QDs , based on the one-dimensional simulation from Figure 2, where the WL-state is situated 108 meV above the first s-state of the QD and still below the p-state of the QD (206 meV above the s-state), are shown in Figure 5a. The WL is charged and discharged via tunneling through the ionized donors from the WL back contact. Compared to the QD, the WL has a shorter tunneling distance, and the electrons thus have a higher probability of tunneling into the WL. Additionally, the occupancy of ionized donor states is strongly temperature-dependent. With higher temperatures, the electrons can occupy ionized donor states above the conduction band, thereby shortening the tunnel distance to the QD and WL, which results in a shift in the base capacitance. At lower temperatures, the occupancy of ionized donor states diminishes and increases the tunnel distance, which accounts for the suppression of the signal below 200 K in Figure 3a. Figure 5b shows a schematic of the energetic quantum states of the QD, the WL, and the WL back contact for an applied gate voltage V_G of -2 V (black), where the QDs are empty and 1 V (red), where the QDs are filled through the WL in an equilibrium state. Due to the different lever arm λ of the QDs and WL, the energetic quantum states shift differently with applied gate voltage. The QDs with a lower λ of 4.1 and the subensemble with λ of 3.5 shift much faster than the WL with higher λ of 7.2. This results in a non-equilibrium resonant condition for each QD quantum state with the WL at different gate voltages, where the WL loses electrons to the back contact. In Figure 5b is the case shown for the s_1 state in darker red, where the occupied quantum state is in resonance with the WL, and the electron can tunnel back and forth, generating the differential capacitance signal. The hysteresis in the C(V) measurement can be explained by this three-level system of QD, WL, and back contact. At higher temperatures, the ground capacitance increases, and the discharging signal remains constant since the QDs are filled for the 250 K signal. The difference spectrum in the inset of Figure 3a then decreases for temperatures above 250 K. Additionally, several mechanisms of defect-assisted transport can play a role here: Frenkel-Poole at high temperatures, electric field enhanced thermal emission, and Fowler-Nordheim assisted tunneling due to the electric field, which is summarized in the review for leakage currents in GaN diodes.[29]

To extract the Coulomb blockade energy E_C from the C(V) measurements, we convert the voltage scale into an energy scale with the before-mentioned equation 1. The energetic distances between the peaks of the C(V) shown in Figure 3b are shown in Table II. To account for the parallel WL shift,

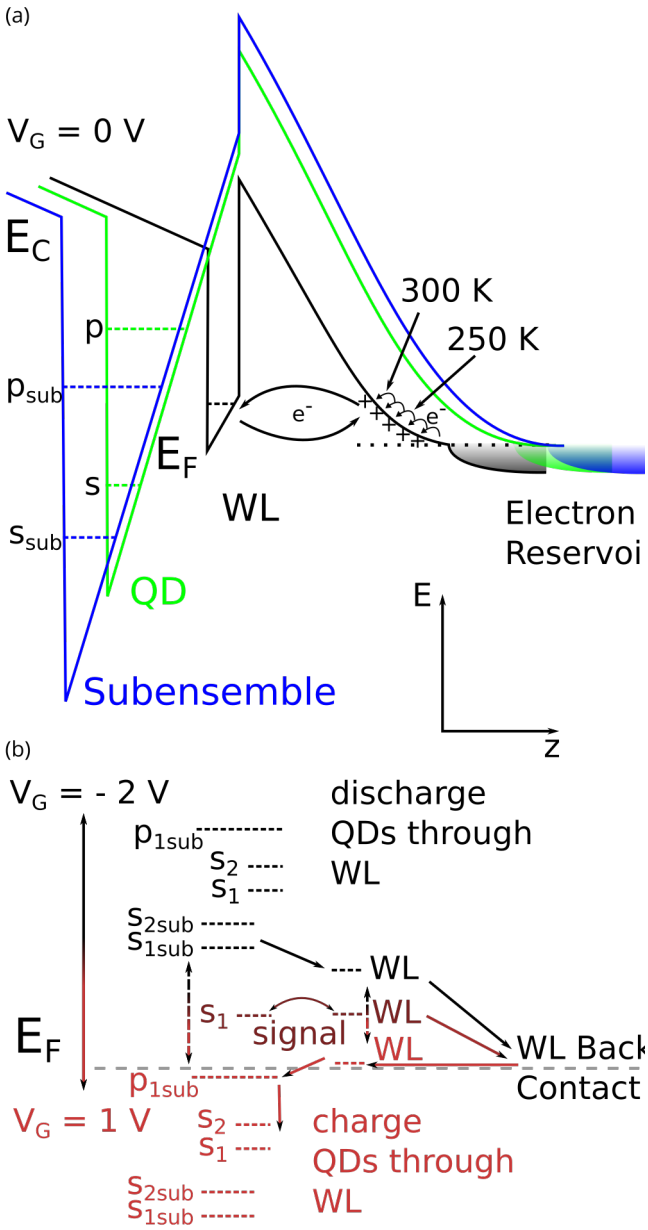

FIG. 5. (a) Schematic band structure for 0 V applied gate voltage of WL (black), QD (green), and subensemble (blue). QD energy states are simplified. Ionized donors are illustrated as plus signs and occupancy of electrons (curved arrows) is thermally activated. The electron reservoir is shown for WL, QD, and subensemble, respectively. (b) Energy states of QD, subensemble, and WL is shown for -2 V gate voltage (black) and 1 V gate voltage (red). An in between case (dark red) is shown when s_1 is in resonance with the WL, which produces the C(V) signal for the s_1 state.

we have to subtract the energetic peak separation with the WL shift between the peaks, which increases the peak separation. We measured the energy spacing of s_{2sub} and p_{1sub} to be 187 meV in the C(V) for 250 K. We consider this signal as this is the largest signal with the p_{1sub} peak present. Taking into account the 28 meV excitonic binding energy[30] reduction

TABLE II. Energy spacing between peaks in the C(V) for 300 K and 250 K. E_C is the Coulomb blockade energy, the spacing between the s_1 and s_2 peak , $\Delta(s_1, s_{1sub})$ the energy spacing between $E(s_1)$ and $E(s_{1sub})$, and $\Delta_{sub}(s_2, p_1)$ the energy spacing between $E(s_{2sub})$ and $E(p_{1sub})$.

Temp [K]	$\Delta(s_1, s_{1sub})$	$E_{C,sub}$	E_C	$\Delta_{sub}(s_2, p_1)$
300	270	120	100	-
250	306	145	129	385
		WL corrected		
300	166	58	57	-
250	177	71	73	187

in the PL and the 50 K temperature difference of the signals, we are in congruity between the PL and C(V) measurements. The one-dimensional simulation is governed by the electric field in the z-direction[22] and is calculated in the effective-mass approximation. The energy separation from the simulation is in accordance with the C(V) measurement as well. Furthermore, the measured energetic distance of s_1 and s_2, the Coulomb blockade energy E_C, equals 71 meV and 73 meV for the subensemble and main ensemble, respectively. This value is much higher than the 20 meV E_C in InAs QDs. Due to the strong localization and the smaller dielectric constant in GaN QDs, a factor of three higher is expected[31], which is in qualitative agreement with our observation.

The non-resonant coupling of QD-states and the back contact through the WL intermediate state and ionized donors have not been observed so far and turn out to be crucial in this study for the coupling between the QDs and the back contact. It shows the importance of engineering the band alignment and the difficulties of single charge transfer at room temperature. Our volume doped GaN samples showed an ionized donor occupancy freeze-out at low temperatures, which inhibited the charging of the QDs. This could be counteracted by coupling the QDs with a two-dimensional electron gas as a back contact whose depletion width is fixed and clearly defined. Further investigations, such as DLTS measurements and the proposed new heterostructure, can bring more insight into the coupling mechanism.

In conclusion, we successfully observed quantum effects at room temperature in C(V) spectroscopy in w-GaN QDs in the form of single-electron charging of the lowest quantum states of the QDs. The PL measurement and the C(V) measurements both indicate a subensemble. A Coulomb blockade energy of around 70 meV for both ensembles was measured successfully at room temperature. Compared to the thermal energy k_BT of the ambient temperature of 25 meV, the higher Coulomb blockade shows the possibility of using quantum effects in GaN QDs at room temperature, in both electronic (single-charge control) and photonic systems (single-photon emission). Electronic applications include multi-valued electronic switches, memory devices, and extremely sensitive charge sensors. In the perspective of photonic applications, if the signal-to-noise-ratio is brought to a sufficient value and with reduced QD-densities, we will perform Hanbury Brown

and Twiss measurements on single QDs.

ACKNOWLEDGMENTS

We gratefully acknowledge the financial support of the Friedrich-Ebert Foundation and the German-French-University DFH/UFA within the CDFA-05-06. This research was funded by ANR Project (ANR-14-CE26-0025) "NANOGANUV" and also supported by GANEX (ANR-11-LABX-0014). GANEX belongs to the publicly funded "Investissements d'Avenir" program managed by the French ANR agency. I gratefully acknowledge fruitful discussions with İsmail Bölükbaşı and Marcel Schmidt, and Nikolai Bart for literary corrections.

DATA AVAILABILITY STATEMENT

The data that support the findings of this study are available from the corresponding author upon reasonable request.

[1] D. V. Talapin and J. Steckel, "Quantum dot light-emitting devices," MRS Bulletin **38**, 685–691 (2013).

[2] I. Buluta, S. Ashhab, and F. Nori, "Natural and artificial atoms for quantum computation," Reports on Progress in Physics **74** (2011), 10.1088/0034-4885/74/10/104401, arXiv:1002.1871.

[3] L. Zhai, M. C. Löbl, G. N. Nguyen, J. Ritzmann, A. Javadi, C. Spinnler, A. D. Wieck, A. Ludwig, and R. J. Warburton, "Low-noise GaAs quantum dots for quantum photonics," Nature Communications **11**, 1–8 (2020), arXiv:2003.00023.

[4] A. Greilich, D. R. Yakovlev, A. Shabaev, A. L. Efros, I. A. Yugova, R. Oulton, V. Stavarache, D. Reuter, A. Wieck, and M. Bayer, "Mode locking of electron spin coherences in singly charged quantum dots," Science **313**, 341–345 (2006).

[5] P. Dimitrakis, P. Normand, C. Bonafos, E. Papadomanolaki, and E. Iliopoulos, "GaN quantum-dots integrated in the gate dielectric of metal-oxide-semiconductor structures for charge-storage applications," Applied Physics Letters **102**, 1–5 (2013).

[6] A. Marent, T. Nowozin, M. Geller, and D. Bimberg, "The QD-flash: A quantum dot-based memory device," Semiconductor Science and Technology **26** (2011), 10.1088/0268-1242/26/1/014026.

[7] S. Kako, C. Santori, K. Hoshino, S. Götzinger, Y. Yamamoto, and Y. Arakawa, "A gallium nitride single-photon source operating at 200K," Nature Materials **5**, 887–892 (2006).

[8] M. J. Holmes, K. Choi, S. Kako, M. Arita, and Y. Arakawa, "Room-temperature triggered single photon emission from a III-nitride site-controlled nanowire quantum dot," Nano Letters **14**, 982–986 (2014).

[9] M. J. Holmes, S. Kako, K. Choi, M. Arita, and Y. Arakawa, "Single Photons from a Hot Solid-State Emitter at 350 K," ACS Photonics **3**, 543–546 (2016).

[10] H. T. Chou, D. Goldhaber-Gordon, S. Schmult, M. J. Manfra, A. M. Sergent, and R. J. Molnar, "Single-electron transistors in GaN/AlGaN heterostructures," Applied Physics Letters **89**, 2004–2007 (2006).

[11] T. Nakaoka, S. Kako, Y. Arakawa, and S. Tarucha, "Coulomb blockade in a self-assembled GaN quantum dot," Applied Physics Letters **90**, 1–4 (2007).

[12] R. Songmuang, G. Katsaros, E. Monroy, P. Spathis, C. Bougerol, M. Mongillo, and S. De Franceschi, "Quantum transport in GaN/AlN double-barrier heterostructure nanowires," Nano Letters **10**, 3545–3550 (2010), arXiv:1005.3637.

[13] V.-T. Rangel-Kuoppa, G. Chen, and W. Jantsch, "Electrical study of self-assembled Ge Quantum Dots embedded in p-type Silicon. Temperature dependent Capacitance Voltage and DLTS study," Solid State Phenomena **178-179**, 67–71 (2011).

[14] L. Wu, M. Dai, X. Huang, Y. Zhang, W. Li, J. Xu, and K. Chen, "Room temperature electron tunneling and storage in a nanocrystalline silicon floating gate structure," Journal of Non-Crystalline Solids **338-340**, 318–321 (2004).

[15] T. Huault, J. Brault, F. Natali, B. Damilano, D. Lefebvre, L. Nguyen, M. Leroux, and J. Massies, "Blue-light emission from GaN Al0.5 Ga0.5 N quantum dots," Applied Physics Letters **92**, 3–6 (2008).

[16] J. Brault, T. Huault, F. Natali, B. Damilano, D. Lefebvre, M. Leroux, M. Korytov, and J. Massies, "Tailoring the shape of GaN/AlxGa1-xN nanostructures to extend their luminescence in the visible range," Journal of Applied Physics **105** (2009), 10.1063/1.3075899.

[17] B. Ofuonye, J. Lee, M. Yan, C. Sun, J.-m. Zuo, and I. Adesida, "Electrical and microstructural properties of thermally annealed Ni/Au and Ni/Pt/Au Schottky contacts on AlGaN/GaN heterostructures," Semiconductor Science and Technology **29** (2014), 10.1088/0268-1242/29/9/095005.

[18] H. Drexler, D. Leonard, W. Hansen, J. P. Kotthaus, and P. M. Petroff, "Spectroscopy of quantum levels in charge-tunable InGaAs quantum dots," Physical Review Letters **73**, 2252–2255 (1994).

[19] T. Xu, L. Zhou, Y. Wang, A. S. Özcan, K. F. Ludwig, D. J. Smith, and T. D. Moustakas, "GaN quantum dot superlattices grown by molecular beam epitaxy at high temperature," Journal of Applied Physics **102** (2007), 10.1063/1.2787155.

[20] D. A. Miller, D. S. Chemla, T. C. Damen, A. C. Gossard, W. Wiegmann, T. H. Wood, and C. A. Burrus, "Band-edge electroabsorption in quantum well structures: The quantum-confined stark effect," Physical Review Letters **53**, 2173–2176 (1984).

[21] M. Korytov, M. Benaissa, J. Brault, T. Huault, T. Neisius, and P. Vennéguès, "Effects of capping on GaN quantum dots deposited on Al0.5 Ga0.5 N by molecular beam epitaxy," Applied Physics Letters **94**, 1–4 (2009).

[22] A. D. Andreev and E. P. O'Reilly, "Theory of the electronic structure of GaN/AlN hexagonal quantum dots," Physical Review B - Condensed Matter and Materials Physics **62**, 15851–15870 (2000).

[23] D. Elmaghraoui, M. Triki, S. Jaziri, G. Muñoz-Matutano, M. Leroux, and J. Martinez-Pastor, "Excitonic complexes in GaN/(Al,Ga)N quantum dots," Journal of Physics Condensed Matter **29** (2017), 10.1088/1361-648X/aa57d5.

[24] S. Birner, "Nextnano Software (www.nextnano.com),".

[25] W. Lei, M. Offer, A. Lorke, C. Notthoff, C. Meier, O. Wibbelhoff, and A. D. Wieck, "Probing the band structure of InAsGaAs quantum dots by capacitance-voltage and photoluminescence spectroscopy," Applied Physics Letters **92**, 1–4 (2008).

[26] R. J. Warburton, B. T. Miller, C. S. Dürr, C. Bödefeld, K. Karrai, J. P. Kotthaus, G. Medeiros-Ribeiro, P. M. Petroff, and S. Huant, "Coulomb interactions in small charge-tunable quantum dots: A simple model," Physical Review B **58**, 16221–16231 (1998).

[27] R. J. Luyken, A. Lorke, A. O. Govorov, J. P. Kotthaus, G. Medeiros-Ribeiro, and P. M. Petroff, "The dynamics of tunneling into self- assembled InAs dots," Applied Physics Letters **74**, 2486 – 2488 (1999).

[28] S. R. Valentin, J. Schwinger, P. Eickelmann, P. A. Labud, A. D. Wieck, B. Sothmann, and A. Ludwig, "Illumination-induced nonequilibrium charge states in self-assembled quantum dots," Physical Review B **97**, 1–7 (2018), arXiv:1710.07545.

[29] A. Syahirah, N. Muridan, and N. Fadzlin, "REVIEW ARTICLE A review of leakage current mechanism in nitride based light emitting diode," Malaysian Journal of Fundamental and Applied Sciences **12**, 77–84 (2016).

[30] B. Monemar, "Fundamental energy gap of gan from photoluminescence excitation spectra," Physical Review B **10**, 676–681 (1974).

[31] D. P. Williams, A. D. Andreev, D. A. Faux, and E. P. O'Reilly, "Surface integral determination of built-in electric fields and analysis of exciton binding energies in nitride-based quantum dots," Physica E: Low-Dimensional Systems and Nanostructures **21**, 358–362 (2004).